Title

Inducible nitric oxide synthase (iNOS)-activated Cxcr2 signaling in myeloid cells promotes TGFβ-dependent squamous cell carcinoma lung metastasis.

Authors

Li, Xing
Ke, Yao
Hernandez, Ariel
et al.

Publication Date

2023-08-28

DOI

10.1016/j.canlet.2023.216330

Peer reviewed

HHS Public Access
Author manuscript
Cancer Lett. Author manuscript; available in PMC 2024 August 28.

Published in final edited form as:
Cancer Lett. 2023 August 28; 570: 216330. doi:10.1016/j.canlet.2023.216330.

Inducible nitric oxide synthase (iNOS)-activated Cxcr2 signaling in myeloid cells promotes TGFβ-dependent squamous cell carcinoma lung metastasis

Xing Li[a,b], **Yao Ke**[b], **Ariel L. Hernandez**[b], **Jingjing Yu**[b], **Li Bian**[b], **Spencer C. Hall**[b], **Kyle Nolan**[b], **Jing H. Wang**[c,d], **Christian D. Young**[b,#], **Xiao-Jing Wang**[b,e,#]

[a]Hospital of Stomatology, Jilin University, Changchun, 130021, P.R. China;

[b]Department of Pathology, University of Colorado Anschutz Medical Campus, Aurora, CO 80045, USA;

[c]Department of Immunology and Microbiology, University of Colorado Anschutz Medical Campus, Aurora, CO 80045, USA;

[d]UPMC Hillman Cancer Center, Department of Medicine, University of Pittsburgh, Pittsburgh, PA, 15213, USA;

[e]Department of Pathology & Laboratory Medicine, University of California Davis, Sacramento, CA 95817, USA;

Abstract

Transforming growth factor beta (TGFβ) activity is linked to metastasis in many cancer types, but whether TGFβ activity is necessary for squamous cell carcinoma (SCC) lung metastasis has not been studied. Here we used a lung metastatic SCC model derived from *keratin 15 (K15)*. *Kras*^{G12D}.*Smad4*$^{-/-}$ SCC and human SCC specimens to identify metastasis drivers and test therapeutic interventions. We demonstrated that a TGFβ receptor (TGFβR) inhibitor reduced lung metastasis in mouse SCC correlating with reduced CD11b^{+}/Ly6G^{+} myeloid cells positive for inducible nitric oxide synthase (iNOS). Further, TGFβ activity and iNOS were higher in primary human oral SCCs with metastasis than SCCs without metastasis. Consistently, either depleting

[#]**Corresponding Authors**: Christian D. Young, Department of Pathology, University of Colorado Anschutz Medical Campus, 12800 E. 19th Ave, RC1-North, Aurora, CO 80045, USA. Phone: +1 303-724-3093; Fax +1 303-724-4730; christian.young@cuanschutz.edu; Xiao-Jing Wang, Department of Pathology & Laboratory Medicine, University of California Davis, 4645 2nd Ave, Research Building III, Room 3200, Sacramento, CA 95817, USA. Phone 916-734-6485; drxwang@ucdavis.edu.

Authors' contributions

XL performed experiments and analyzed and interpreted data; YK, ALH, SCH, and KN performed experiments; JY and LB performed data analysis and discussed results; XJW, CDY and JHW designed and supervised the study; XL, CDY and XJW wrote the manuscript. All authors read and approved the final manuscript.

Competing interests

The authors declare that they have no competing interests.

Declaration of interests

The authors declare that they have no known competing financial interests or personal relationships that could have appeared to influence the work reported in this paper.

myeloid cells with anti-Gr1 antibody or inhibiting iNOS with L-N6-(1-iminoethyl)-L-lysine (L-NIL) reduced SCC lung metastasis. L-NIL treated tumor-bearing mice exhibited reductions in tumor-infiltrating myeloid cells and in plasma Cxcl5 levels, and attenuated primary tumor growth with increased apoptosis and decreased proliferation. Blocking Cxcl5 with an antagonist of its receptor Cxcr2, SB225002, also reduced SCC lung metastasis.

Keywords

Oral cancer; myeloid-derived suppressor cells; L-NIL; spontaneous lung metastasis model; Smad4 deletion

1. Introduction

Squamous cell carcinoma (SCC) arises from stratified epithelia such as that in the skin and oral cavity. Despite efforts to improve therapeutic approaches, patients with SCC have a 5-year survival rate of 40% to 50% [1]. The worst outcome for SCC is distant metastasis to vital organs, with the lungs being the metastatic site in approximately 80% of cases [2]. Lung metastasis is a multi-step process involving invasion of cancer cells into surrounding tissues, intravasation, survival in the bloodstream, extravasation and proliferation after seeding to the lung [3]. Hence, there is an urgent need to identify new therapeutic targets and treatments for metastatic cancer.

Transforming growth factor beta (TGFβ) is known to be overexpressed in SCC [4]. Although TGFβ is linked to metastasis in many cancer types, the lack of spontaneous metastatic SCC models has limited investigation to determine if TGFβ activation is necessary for metastasis, and if so, if it can be a potential therapeutic target in metastatic SCC. To date, most studies of TGFβ inhibitors have focused primarily on the activation of $CD8^+$ T cells and natural killer cells in the tumor microenvironment (TME) for tumor eradication [5–7]. However, advanced SCC patients are often severely immune suppressed [8, 9] and TGFβ inhibitor effectiveness in SCC metastasis in severely immune compromised conditions has not been directly tested. TGFβ is produced by both tumor cells and stromal cells. However, because TGFβ is a secreted protein and is often activated in the extracellular matrix, it exerts effects on all adjacent cells including tumor cells and stromal cells [10, 11]. Among stromal cells that are also a source of TGFβ, we previously showed cancer associated fibroblasts (CAFs) primarily promote survival of metastatic cells after they reach the metastatic site but not at the primary tumor site [12]. Therefore, we examined tumor-infiltrating myeloid cells in this study because they have been shown to promote TGFβ-dependent metastasis in other tumor types [13].

Myeloid cells are heterogeneous blood cells originating from the bone marrow and are recruited to peripheral sites of inflammation or cancer [14]. Among myeloid cells, tumor-associated macrophages (TAMs) and $CD11b^+/Gr1^+$ myeloid cells, putative myeloid-derived suppressor cells (MDSCs), are the most common subpopulations in tumors [15]. In addition to immune suppression [16], myeloid cells are actively involved in tumor growth, angiogenesis and the metastatic process in many cancer types [17–19]. Our previous study has shown that although TAMs contribute to SCC expansion, they do not significantly

contribute to SCC lung metastasis [20]. This finding highlights tumor-type specific functions of myeloid cells. It remains to be determined how much $CD11b^+/Gr1^+$ myeloid cells or their effectors, including nitric oxide produced by inducible nitric oxide synthase (iNOS) activity [21], contribute to SCC lung metastasis.

We previously developed *keratin 15 (K15)-CrePR. Kras*^{G12D} and *Smad4* deletion (*Smad4*$^{-/-}$) mice that develop spontaneous SCC and lung metastasis [22]. By transplanting SCC cell lines derived from this model to establish SCC and testing experimental therapeutics and using human SCC specimens for validation, we address the following: 1) whether TGFβ signaling contributes to SCC lung metastasis; 2) whether myeloid cells are a major effector of TGFβ-dependent metastasis; 3) identify mechanisms associated with the role of myeloid cells in SCC metastasis. Our study revealed that TGFβR inhibition is sufficient to reduce SCC lung metastasis. TGFβR inhibitor reduced MDSCs but not macrophages, and metastasis was promoted by $iNOS^+$ myeloid cells. Furthermore, the chemokine Cxcl5 was a main target of iNOS inhibition and was critical in TGFβ-induced SCC metastasis. These experiments identified several therapeutic targets related to TGFβ-mediated metastasis, i.e., targeting TGFβ or myeloid cells directly or their downstream effectors, iNOS or Cxcl5/Cxcr2 signaling. Our analysis provides insight into future clinical studies for prognostic markers and therapeutic strategies for treating metastatic SCC.

2. Materials and methods

2.1 Cell lines and mouse models

The mouse SCC cell lines derived from *K15.Kras*^{G12D}*.Smad4*$^{-/-}$ mice, B931 and B866 were developed as previously described [22]. SCC cell lines were cultured in Dulbecco's modified Eagle medium (DMEM) containing 10% fetal bovine serum (FBS) and 1% penicillin.

Animal studies were approved by the University of Colorado AMC Institutional Animal Care and Use Committee (protocol #254). Athymic, 6 to 8 weeks-old nude mice were purchased from Charles River Laboratories. 3,000 B931 or B866 cells were suspended in PBS containing 50% Matrigel (Thermo Fisher Scientific, #CB-40234) to a final volume of 50 μL and injected subcutaneously to the flanks of mice. Tumor cells were implanted onto gender matched mice: B866 onto male mice and B931 onto female mice. Sample size was chosen based on previously published experiments and experience with the size distribution of the tumor cell lines used in this study.

Treatment began when tumors were palpable, approximately 7–12 days post-injection. Tumor volumes were measured with calipers twice a week and calculated as (length × width^2)/2. Mice were euthanized when they experienced >15% weight loss, severe tumor ulceration, or tumors reached 2 cm in diameter. Tumors and spleens were collected for molecular and morphologic analysis after sacrifice. Lung metastases were counted using microscopy.

2.2 *In vivo* treatment

All mice were randomized into two groups to equally distribute small tumor size variations once tumors become palpable, ~7–12 days post-transplantation. Mice were treated daily with 150 mg/kg TGFβ type I receptor kinase inhibitor Galunisertib (LY2157299) (MedChemExpress, #HY- 13226) or vehicle (1% sodium carboxymethylcellulose, 0.5% sodium lauryl sulfate) by oral gavage as previously described [7].

For the depletion of myeloid cells *in vivo*, mice received intraperitoneal injections of 200 μg anti-mouse Gr1 (BioXCell, #BE0075, clone RB6–8C5) or isotype control (BioXCell, #BE0090, clone LTF2) twice a week [23]. 5 mg/kg Cxcr2 antagonist SB225002 (MedChemExpress, #HY16711) or vehicle (10% DMSO, 40% PEG300, 5% Tween-80, 45% saline) was administered by intraperitoneal injection daily [24].

L-N6-(1-iminoethyl)-L-lysine (L-NIL) (MedChemExpress, #HY-12116), iNOS inhibitor, was administered in drinking water at 0.2% continuously through the entire study. Control mice received regular drinking water [25].

2.3 H&E staining

Lungs harvested at study endpoint were embedded in paraffin, sectioned, and stained with Hematoxylin and eosin (H&E). Histopathology of lung metastasis was evaluated using H&E sections. All lung lobes of each mouse were used for counting lung metastasis.

2.4 *In Vivo* Imaging System (IVIS)

Tumor cell lines were stably transduced with a firefly luciferase reporter (CMV, puromycin) (Kerafast, #FCT226). Briefly, cells were treated with lentiviral stocks at an MOI of 10 with 8 μg/mL polybrene then selected with puromycin (2 μg/mL). To detect luciferase activity *in vivo*, mice bearing luciferase-labeled B931 tumors were injected i.p. with 150 mg/kg luciferin 5 minutes before imaging using an IVIS Spectrum system (PerkinElmer) at the University of Colorado Cancer Center Animal Imaging Shared Resource. Lung metastasis was detected and evaluated 5 weeks post transplantation of B931-luciferase cells.

2.5 Immunofluorescence staining

Immunofluorescence staining was performed with tumors collected at the end of each study. Primary antibodies used were: Ly6G (1:50, CST, #87048), CD11b (1:400, Novus, #NB600–1327SS), F4/80 (1:200, CST, #70076), and Cytokeratin (Dako, #M351501–2). Alexa Fluor–conjugated secondary antibodies (Thermo Fisher Scientific) were used for detection. Samples were counterstained with DAPI and coverslipped with Prolong Diamond mounting media (Thermo Fisher).

2.6 Immunohistochemistry

2.6.1 IHC of mouse tissues—All tumor tissues were fixed in 10% neutral-buffered formalin overnight and embedded in paraffin. Sections were de-waxed in xylenes and rehydrated in graded alcohols. Antigen retrieval was achieved using citrate buffer (pH 6.0) for 5 minutes under high pressure. The primary antibodies used were pSMAD2 (1:300, Invitrogen, #44–244G), iNOS (1:500, Novus, #NBP1–33780), Cleaved-caspase 3 (1:200,

CST, #9661), Ki67 (1:400, CST, #12202), Ly6G (1:50, CST, #87048). Stained slides were scanned with an Aperio AT2 scanner (Leica) at the University of Colorado Cancer Center Pathology Shared Resource, and 5 random images per slide were collected at 200X using ImageScope software (Leica). Integrated optical density (IOD; IOD = area × staining intensity) of indicated markers was quantified by Image Pro Plus 7.0. The mean IOD was calculated for all 5 images per sample and used for statistical analysis.

2.6.2 IHC of human oral SCC tissues—Patients enrolled in this study had histologically confirmed oral SCC with or without lymph node metastasis. This study was approved by the Ethical Committee of Jilin University (protocol #14) and complied with all relevant ethical regulations. Written informed consent was obtained from all patients participating in this study. A total of 17 SCC patients were included in this study; eight had non-metastatic SCC and nine had metastatic SCC. Sections of primary tumors were stained with primary antibodies against TGFβ1 (1:400, Abcam, #ab215715), p-SMAD3 (1:500, Bioss, #bs3425R), iNOS (1:800, Proteintech, #22226–1-AP). 5 fields were captured at 200X per sample. IOD of indicated markers in each image were measured by Image Pro Plus 7.0. The mean IOD of 5 fields was the IOD value for one sample.

2.7 Flow cytometry

To characterize immune cell infiltration, single cell suspensions were prepared from tumors and spleen tissues. Tumors were minced with scalpels, dissociated in Miltenyi gentleMACS C tubes on a Miltenyi gentleMACS Dissociator and digested with collagenase II (Worthington, #LS004204) for 40 minutes at 37°C. Digests were filtered through a 100 μm strainer. Spleens were smashed through a 70 μm strainer using a syringe plunger. The strainer was washed with HBSS to further elute splenocytes. Red blood cells (RBCs) were lysed with RBC lysis buffer (eBioscience, #00–4333-57) for 5 minutes, neutralized with PBS and the remaining cells pelleted by centrifugation. Cells were strained through a 40 μm strainer before counting. To prevent nonspecific binding, cells were incubated at 4°C for 10 minutes with anti-CD16/CD32 to block Fc receptors (BD Biosciences, #553142). One million cells were incubated with fluorescently-labeled surface antibodies for 30 minutes at 4°C. Antibodies used included: CD45 (BD, #564279), CD11b (Biolegend, #101216), Ly6G (Biolegend, #127627), Ly6C (Biolegend, #128033), CXCR2 (BD, #747812). Cell viability was determined using ghost dye 780 (Tonbo Biosciences). Flow cytometry data were acquired on a Bio-Rad YETI instrument at the University of Colorado Cancer Center Flow Cytometry Shared Resource and analyzed using the Kaluza software with fluorescence-minus-one controls to verify gating.

2.8 Mass cytometry (CyTOF)

Single cell suspensions were prepared from tumors and spleens as described for flow cytometry. Following RBC lysis, 3 million cells were incubated in cisplatin for 5 minutes, washed and blocked for FcγR using CD16/CD32 antibody, and incubated with metal-conjugated Fluidigm cell surface antibodies for 30 minutes at room temperature. Antibodies are detailed in Supplementary Table S1. Cells were washed once, fixed with fix/perm buffer for 10 minutes, washed and incubated 30 minutes with metal-conjugated antibodies recognizing cytoplasmic/secreted factors then washed and fixed with 1.6% formaldehyde

for 10 minutes. Resuspended cells were kept in intercalator at 4°C overnight to stain the nuclei. Samples were analyzed on a Helios mass cytometer (Fluidigm) at the University of Colorado Cancer Center Flow Cytometry Shared Resource. An equal number of events for each sample were analyzed using tSNE with FCS Express 7 software. Dead cells were excluded based on positive cisplatin staining, and nucleated cells were confirmed with IR-Dye (Fluidigm). Live, nucleated, $CD45^+$ cells were clustered and gated based on individual marker expression. Markers used to define each cluster are stated in the Supplementary Table S2.

2.9 Detection of nitric oxide (NO) metabolites *in vivo*

Plasma was prepared by centrifugation of whole blood at 1,500xg for 15 min, collecting the top plasma layer away from pelleted cells and stored at −80°C. After thawing, plasma was clarified by passage through a 10 kDa cutoff spin-filter (Millipore, #UFC801024). Nitrite and nitrate levels were determined by Griess assay (Sigma Aldrich, #23479) according to the manufacturer's instructions.

2.10 Cytokine array of plasma and tumor lysates

Proteome Profiler Mouse XL Cytokine Array (RD, #ARY028) was used for detecting cytokines. Briefly, membranes were blocked with blocking buffer at room temperature for 1 h and incubated with plasma (100 μL) or tumor lysates (200 μg) at 4°C overnight and then detection of cytokines was performed following manufacturer's instructions and activity detected on a BioRad ChemiDoc (20 min exposure). The data were digitized and subjected to image analysis (Image J) for quantification.

2.11 Statistical Analysis

Unless otherwise specified, statistical differences between two groups was determined by using Student's t-test or non-parametric Mann-Whitney exact test. Individual data points represent the value of a single biological sample and are shown as mean ± SD unless otherwise indicated. No samples or data were excluded from analysis. Survival curve was determined by the Kaplan–Meier analysis. $P < 0.05$ was considered statistically significant. *, $P < 0.05$; **, $P < 0.01$; ***, $P < 0.001$.

3. Results

3.1 TGFβR inhibitor reduced lung metastasis correlating to reduced $CD11b^+/Ly6G^+$ and $iNOS^+$ cells

We transplanted *K15.Kras*^{G12D}*Smad4*$^{-/-}$ SCC cells (B931 or B866) to the flank of athymic nude mice. These mice developed lung metastasis within 4–5 weeks after transplantation. To determine if TGFβ signaling plays a causal role in SCC lung metastasis, we treated tumor-bearing mice with TGFβR inhibitor (or vehicle control) when the tumors were palpable. TGFβR inhibitor reduced lung metastasis as compared to vehicle-treated control mice (Fig. 1A–B). TGFβR inhibitor reduced pSmad2 staining in primary tumors (Supplementary Fig. S1A), demonstrating on-target activity of the inhibitor. Additionally, primary tumor volumes were not changed by treatment (Supplementary Fig. S1B–C) suggesting tumor size is not correlated with metastasis. Although pSmad2/3 reduction is a readout of TGFβ

inhibitor activity in tumor cells and stromal cells, tumor cells do not have canonical TGFβ signaling because of epithelial-specific *Smad4* deletion in these models, thus canonical TGFβ signaling is present only in stromal cells. CD11b$^+$ myeloid cells were the most abundant immune cells in the tumor microenvironment in our two mouse SCC models (Supplementary Fig. S2) with F4/80$^+$ macrophages and Ly6G$^+$ granulocytes being the most frequent myeloid cell subtypes (Supplementary Fig. S2 and Fig. 1C). Using immunostaining, we found that Ly6G$^+$ cells, but not F4/80$^+$ cells, were reduced significantly in the primary SCC of TGFβR inhibitor-treated mice (Fig. 1D–E), correlating with reduced lung metastasis.

iNOS is known to be produced by myeloid cells and tumor cells [26, 27]; CyTOF analysis revealed that iNOS was expressed in some CD11b$^+$ myeloid cells and tumor cells in B931 tumors (Fig. 1F). To further explore if iNOS is induced by TGFβ, we stained iNOS in B931 and B866 tumor tissue. TGFβR inhibitor reduced iNOS$^+$ cells (Fig. 1G).

To assess if our findings in mouse models apply to human SCC, we performed IHC staining of TGFβ1, p-SMAD3, and iNOS in primary oral SCC clinical specimens from patients with or without metastasis. Because biopsy of oral SCC lung metastasis in patients is not feasible, we examined primary SCC from patients with and without lymph node metastasis. Staining of these proteins in primary SCCs from patients with metastasis were significantly higher than in SCC patients without metastasis (Fig. 1H–I), leading to the hypothesis that TGFβ1 and iNOS in primary SCC are critical regulators of metastasis. TGFβ1, pSMAD3 and iNOS were expressed in both tumor cells and some stromal cells in human oral squamous cell carcinoma (OSCC) samples consistent with published results [10, 12, 28, 29].

3.2 Myeloid cell depletion suppressed SCC lung metastasis

Based on the above results, we sought to determine if non-F4/80$^+$ myeloid cells or iNOS activity are contributors to lung metastasis. Given that a previous report showed that Gr1$^+$ myeloid cells contribute to TGFβ-mediated metastasis in breast cancer [13], we used anti-Gr1 (Ly6G/Ly6C) neutralizing monoclonal antibody or isotype control antibody to treat tumor-bearing mice. Depletion of myeloid cells with anti-Gr1 significantly reduced B931 and B866 SCC lung metastasis (Fig. 2A), but did not alter primary tumor growth (Supplementary Fig. S3A). Further, anti-Gr1 depleted CD11b$^+$Ly6G$^+$ myeloid cells in both B931 (Fig. 2B–D) and B866 (Supplementary Fig. S3B–D) tumor bearing mice, evidenced by significantly decreased CD11b$^+$Ly6G$^+$ cells in tumors and spleens with anti-Gr1 treatment. These results show that Gr1$^+$ myeloid cells in the tumor-bearing mice are a major contributor to SCC lung metastasis but not tumor growth.

3.3 iNOS inhibition suppressed SCC lung metastasis

To assess the role of iNOS in SCC lung metastasis, we treated tumor-bearing mice with L-NIL, an inhibitor of iNOS [25]. L-NIL-treated mice bearing B931 or B866 tumors had markedly reduced lung metastasis compared with control groups (Fig. 3A–C). Similarly, in B931-luciferase tumor-bearing mice treated with vehicle control, there was obvious lung metastasis as observed by bioluminescent IVIS imaging in 60% of mice whereas L-NIL treated mice had no visible lung metastasis (Fig. 3D).

3.4 Tumor Ly6G$^+$ myeloid cell accumulation was reduced with iNOS inhibitor

Myeloid cell iNOS activity is critical to myeloid cell function [27]. To determine how iNOS inhibition influenced tumor Ly6G$^+$ cells, we performed IHC staining and flow cytometry. Total infiltrated Ly6G$^+$ myeloid cell numbers were reduced with L-NIL treatment relative to control, as shown by IHC staining and quantification of Ly6G$^+$ cells in B931 primary tumor sections (Fig. 4A). Flow cytometry analysis validated that the percentage of Ly6G$^+$ myeloid cells was reduced in L-NIL treated B931 tumor bearing mice (Fig. 4B). The effect of L-NIL treatment on Ly6G$^+$ cells in B866 tumors was similar to that observed in B931 tumors (Fig. 4C and Supplementary Fig. S4A).

We also performed CyTOF analysis of spleen cells from tumor-bearing mice to screen for changes in CD45$^+$ leukocyte populations after L-NIL treatment. However, there were no changes in spleen cell populations relative to vehicle control group (Supplementary Fig. S4B–C), indicating L-NIL primarily affected the TME. Direct analysis of CD11b$^+$Ly6G$^+$ spleen cells using flow cytometry also demonstrated no difference between L-NIL treated and control treated mice (Supplementary Fig. S4D–E).

3. 5 Cxcl5/Cxcr2 blockade reduced myeloid cell infiltration and SCC lung metastasis

To identify molecular mediators associated with reduced Ly6G$^+$ myeloid cells in SCC bearing mice treated with L-NIL, plasma was analyzed using a cytokine antibody array. Among down-regulated cytokines associated with L-NIL treatment in analyzed plasma samples, three molecules related to metastasis were the top candidates in both tumor types: intracellular cell adhesion molecular 1 (Icam1), Matrix Metalloproteinase 2 (Mmp2) and Cxcl5 (Fig. 5A–D). Cxcl5 is a key chemokine involved in myeloid cell recruitment and was decreased significantly in the plasma of both B931 and B866 tumor bearing mice treated with L-NIL (Fig. 5B,D). Cytokine array analysis of tumor lysates showed metastasis mediators such as Icam1, Mmp2, Mmp3 and Mmp9 reduced with L-NIL treatment (Supplementary Fig. S5A–D).

Cxcr2 is the receptor for Cxcl5. Flow cytometry of dissociated B931 tumors showed 90% of Ly6G$^+$ myeloid cells expressed Cxcr2 on the cell surface (Fig. 5E). To determine whether Cxcl5/Cxcr2 signaling played a functional role in recruitment of myeloid cells into the SCC TME and influenced metastasis, we treated tumor-bearing mice with Cxcr2 inhibitor SB225002, “Cxcr2i”. SB225002 reduced infiltration of Ly6G$^+$ myeloid cells in B931 and B866 tumors (Fig.5F and Supplementary Fig. S6A). Similar to mice treated with anti-Gr1 neutralizing antibody, SB225002-treated mice also showed significant reduction in lung metastasis compared with the vehicle (Fig. 5G–H). Cxcr2 antagonist SB255002 did not affect primary tumor growth (Supplementary Fig. S6B–C). Thus, Cxcr2 antagonist SB255002 also inhibited myeloid cells infiltration in the primary tumor and reduced lung metastasis.

3.6 L-NIL treatment reduced proliferation and increased apoptosis of tumor cells

In addition to reducing lung metastasis, L-NIL significantly reduced both B931 and B866 tumor volume (Fig. 6A–B), which may be attributed to an indirect effect via myeloid cells or a direct effect on tumor cells because tumor cells also express iNOS (Fig. 1).

We assessed if reduced tumor growth in L-NIL treated animals was due to decreased proliferation or increased cell death. Ki67 staining of proliferating cells was reduced in L-NIL-treated B931 and B866 tumors (Fig. 6C–D). Further, cleaved-caspase3 (C-caspase3) positive apoptotic cells were increased with L-NIL treated tumors compared with control in both B931 and B866 tumors (Fig. 6C–D). Nitric oxide (NO) is a potent bioactive molecule produced by iNOS; downstream effects of endogenous NO in cancer include evasion of apoptosis, enhanced proliferation and metastatic process [29]. To verify if nitric oxide metabolites are affected by L-NIL treatment and may contribute to decreased proliferation and increased apoptosis with L-NIL, we examined tumor-bearing mouse plasma for nitric oxide metabolites using a Nitrite/Nitrate assay. Total nitric oxide metabolite concentration was higher in tumor bearing mice compared with naïve mice, and the concentration was reduced significantly with L-NIL treatment in both B931 and B866 tumors compared with control (Fig. 6E). Lastly, L-NIL prolonged survival of B866 tumor bearing mice (Fig. 6F), while long-term survival of B931 tumor bearing mice was precluded from study due to tumor size constraints requiring euthanasia.

4. Discussion

TGFβR inhibitor reduced lung metastasis correlating to reduced CD11b$^+$/Ly6G$^+$ myeloid cells

Our previous study has shown that TGFβ activation is higher in primary human SCC with lung metastasis than SCC without lung metastasis [12]. TGFβR inhibitor treatment reduced SCC lung metastasis in the absence of T cells (Fig. 1), suggesting that non-T cell targets contribute to TGFβ-mediated SCC metastasis. Using CyTOF, we screened infiltrated leukocytes in *Kras*^{G12D}.*Smad4*$^{-/-}$ SCCs (Fig. 1). The majority of CD45$^+$ cells were CD11b$^+$ cells. Our current study, using pharmacologic inhibitors, demonstrated that myeloid cells are the major effector of TGFβ induced lung metastasis. This notion is supported by data demonstrating TGFβR inhibitor suppressed lung metastasis with reduced CD11$^+$/Ly6G$^+$ myeloid cells (Fig. 1). Further, depletion of myeloid cells with anti-Gr1 inhibited lung metastasis to an extent similar to TGFβR inhibitor (Fig. 2).

Our results suggesting that myeloid cells facilitate SCC lung metastasis are consistent with those reported in other cancer types [30–33]. For example, TGFβ in myeloid cells promoted breast cancer lung metastasis and genetic deletion of Tgfbr2 specifically in myeloid cells decreased tumor metastasis [13]. Myeloid cells were previously implicated in supporting tumor cell invasion by releasing high amounts of degrading enzymes such as matrix metalloproteinase (MMPs). MMP2, MMP3, and MMP9 digest extracellular matrix (ECM) allowing tumor cells to migrate [32]. While myeloid cells were reported to promote SCC growth in syngeneic immunocompetent models [25], primary SCC growth in our model was not affected by myeloid cell depletion with anti-Gr1. It is possible that those effects are T cell dependent and thus did not occur in an immune compromised background. Because advanced SCCs can induce severe immune suppression and SCCs occur at a higher rate in immune compromised patients [8, 9, 34], our study's identification of a T cell-independent role of myeloid cells in SCC metastasis in immune compromised mice is a critical point for further investigation.

iNOS inhibition with L-NIL suppressed SCC lung metastasis and growth— The reduction of iNOS$^+$ cells in tumors from TGFβ inhibitor treated mice suggests that iNOS might be an effector contributing to TGFβ induced lung metastasis (Fig. 1). This is supported by reduction of lung metastasis with iNOS inhibitor (Fig. 3). Because myeloid cells are a major source of iNOS in tumors (Fig. 1), the reduction of myeloid cells by TGFβ inhibitor may be responsible for the decrease in iNOS$^+$ cells overall. The role of iNOS/NO in cancer development and progression appears contradictory among various tumor types and is less well known in SCC [29, 35]. Studies employing inhibition or genetic deletion of iNOS show that iNOS/NO can both promote or inhibit tumor progression and metastasis [21, 36]. The effects of iNOS/NO in tumors seems to depend on the activity and origin of iNOS/NO, concentration and duration of NO exposure, and cellular sensitivity to NO [21]. Previous reports have demonstrated a correlation between high iNOS expression and poor prognosis in patients with oral cancer [37, 38]. However, given the limited experimental SCC metastasis models, it remained to be determined if iNOS production contributed to SCC lung metastasis. In this study, we showed that iNOS inhibitor L-NIL reduced SCC lung metastasis. Nitric oxide is the main effector produced by iNOS activity, which is involved in tumor cell invasion and metastasis [29]. Nitric oxide metabolites nitrite and nitrate were reduced with L-NIL (Fig. 6), indicating that the lower capacity of cancer cell migration and invasion correlates with NO metabolite levels and likely reflects iNOS activity.

The tumor immune microenvironment was remodeled in L-NIL treated mice. It is reported that Ly6G$^+$ myeloid cells promote cancer cell metastasis via immune-independent routes such as ECM remodeling [39]. Obvious reduction of Ly6G$^+$ myeloid cells was observed in SCC-bearing mice treated with L-NIL (Fig. 4). It has been reported that MMPs regulate tumor growth, invasion, and metastasis [40]. In our study, we observed that invasion related molecules Mmp2 and Mmp3 were reduced in tumor lysates and/or plasma from mice treated with L-NIL (Fig.5 and Supplementary Fig. S5), suggesting that lower metastasis rates in L-NIL treated mice may be linked to Mmp levels and activity; this requires validation. Additionally, Icam1 aids cancer cell adherence to the endothelium and contributes to distant metastasis [41, 42]; Icam1 was also decreased with L-NIL treatment (Fig.5), suggesting this could be a mechanism for decreased tumor cells in circulation and metastasis. Because we did not observe significant changes in spleen immune cell numbers, our data suggests that the L-NIL effect is unique to the TME.

Decreased tumor growth in L-NIL treated mice was due to increased apoptosis and decreased proliferation. Our data are consistent with a previous study that shows L-NIL reduced tumor growth in melanoma and increased apoptotic cells [43]. iNOS is expressed in myeloid cells (Fig. 1), so increased cell death in tumors of L-NIL treated mice may be via changes in myeloid cell function or a lack of myeloid cells to sustain tumor maintenance. Alternatively, there might be a direct effect because some tumor cells also expressed iNOS, which can promote proliferation [44, 45] and could be inhibited with L-NIL. Decreased tumor growth could be a mechanism of reduced metastasis because tumor size often correlates with metastasis [46], but the effects of L-NIL on metastasis were more dramatic than the effect on tumor size, and TGFβi, anti-Gr1 and Cxcr2 inhibition treatments prevented metastasis without affecting tumor size, reinforcing the conclusion that tumor

myeloid cells play a direct role in metastasis independent of tumor size. Thus, the decreased tumor growth observed with L-NIL treatment is likely a direct effect on tumor cells.

Cxcl5/Cxcr2 signaling mediated Ly6G$^+$ myeloid cell infiltration and promoted lung metastasis—In plasma from B931 and B866 tumor-bearing mice, we found striking downregulation in the levels of Cxcl5 in mice treated with L-NIL treatment (Fig. 5). Cxcl5 chemokine plays a key role in the efficient recruitment of Ly6G$^+$ myeloid cells [24, 47]. Cxcl5 can be secreted by primary tumor cells and cells in the TME, including fibroblasts and myeloid cells [48]. Cxcl5 could be a major target of L-NIL and L-NIL might contribute to the reduction of Cxcl5 via regulating tumor cell and/or myeloid cell Cxcl5 expression.

Cxcr2 is the receptor for Cxcl5 [48] and ~90% of Ly6G$^+$ cells express Cxcr2 on the cell surface (Fig. 5). Cxcr2 signaling mediated myeloid cell infiltration and tumor growth in immunocompetent prostate and gastric cancer models [16, 24]. In contrast, we found there were no changes in tumor growth with either Cxcr2 antagonist or anti-Gr1 treatment, but tumor growth rate was decreased with L-NIL treatment. Perhaps L-NIL is having a direct effect on iNOS expressing tumor cells (and myeloid cells) while anti-Gr1 and Cxcr2 are myeloid-restricted targets. It is also possible that the influence of myeloid cells on tumor growth is T cell-dependent and there is no effect in our immune compromised SCC model. The effectiveness of targeting Cxcr2 and anti-Gr1 in our model suggests targeting mechanisms that specifically regulate Ly6G$^+$ myeloid cell recruitment would provide therapeutic benefit for patients with metastatic cancer or targeting iNOS may influence both tumor cells and myeloid cells, decreasing both tumor progression and metastasis.

In summary, we provided evidence that iNOS and Gr1$^+$ myeloid cells are major contributors to TGFβ-mediated lung metastasis. iNOS inhibitor L-NIL inhibited SCC lung metastasis and reduced Cxcl5 induced myeloid cell infiltration (Fig.7). Because TGFβR inhibitor, anti-Gr1, L-NIL, and Cxcr2 antagonist all reduced primary tumor myeloid cell abundance and lung metastasis in an immune compromised background, our studies suggest that these therapeutic agents could be beneficial in patients with suppressed immune systems, which is common in later stage SCC patients. While the use of pharmacologic inhibitors is translational and common in cancer treatment, genetic studies to narrow the contributions of TGFβ1, Cxcl5 and iNOS to different myeloid cell populations or tumor cell populations to metastasis would help define the cellular and molecular players and suggest more precise drug targets or cellular diagnostics. Future studies are warranted to evaluate if these therapeutic agents in immune-competent conditions elicit even stronger efficacy against SCC metastasis.

Supplementary Material

Refer to Web version on PubMed Central for supplementary material.

Acknowledgements

We thank Xueke Shi for her assistance in samples collection, Khoa Nguyen for technical assistance in data analysis and Pamela Garl for critical proof reading.

Funding

This work was supported by NIH grants DE027329, DE028420 and P50CA261605. Xing Li was supported by the State Scholarship Fund of China Scholarship Council (No.201908210300). The University of Colorado Cancer Center shared resources used in these studies (Flow Cytometry Shared Resource, Pathology Shared Resource and Animal Imaging Shared Resource) are supported by Cancer Center Support Grant P30CA046934.

Availability of data and materials

The datasets used and/or analyzed during the current study are available from the corresponding author on reasonable request.

Abbreviations

C-caspase3	Cleaved-caspase3
CAFs	Cancer associated fibroblasts
ECM	Extracellular matrix
ICAM1	Intracellular cell adhesion molecular 1
iNOS	Inducible nitric oxide synthase
IVIS	*In vivo* imaging system
K15	Keratin 15
L-NIL	L-N6–1-iminoethyl-L-lysine
MDSCs	Myeloid-derived suppressor cells
MMP	Matrix Metalloproteinase
NO	Nitric oxide
OSCC	Oral Squamous Cell Carcinoma
RBC	Red blood cell
SCC	Squamous cell carcinoma
TAMs	Tumor associated macrophages
TGFβ	Transforming growth factor beta
TGFβR	TGFβ receptor
TME	Tumor microenvironment

References

[1]. Leemans CR, Braakhuis BJ, Brakenhoff RH, The molecular biology of head and neck cancer, Nature reviews. Cancer, 11 (2011) 9–22. [PubMed: 21160525]

[2]. Bohnenberger H, Kaderali L, Ströbel P, Yepes D, Plessmann U, Dharia NV, Yao S, Heydt C, Merkelbach-Bruse S, Emmert A, Hoffmann J, Bodemeyer J, Reuter-Jessen K, Lois AM, Dröge

LH, Baumeister P, Walz C, Biggemann L, Walter R, Häupl B, Comoglio F, Pan KT, Scheich S, Lenz C, Küffer S, Bremmer F, Kitz J, Sitte M, Beißbarth T, Hinterthaner M, Sebastian M, Lotz J, Schildhaus HU, Wolff H, Danner BC, Brandts C, Büttner R, Canis M, Stegmaier K, Serve H, Urlaub H, Oellerich T, Comparative proteomics reveals a diagnostic signature for pulmonary head-and-neck cancer metastasis, EMBO molecular medicine, 10 (2018).

[3]. Chaffer CL, Weinberg RA, A perspective on cancer cell metastasis, Science (New York, N.Y.), 331 (2011) 1559–1564. [PubMed: 21436443]

[4]. Derynck R, Turley SJ, Akhurst RJ, TGFβ biology in cancer progression and immunotherapy, Nature reviews. Clinical oncology, 18 (2021) 9–34.

[5]. Thomas DA, Massagué J, TGF-beta directly targets cytotoxic T cell functions during tumor evasion of immune surveillance, Cancer cell, 8 (2005) 369–380. [PubMed: 16286245]

[6]. Gao Y, Souza-Fonseca-Guimaraes F, Bald T, Ng SS, Young A, Ngiow SF, Rautela J, Straube J, Waddell N, Blake SJ, Yan J, Bartholin L, Lee JS, Vivier E, Takeda K, Messaoudene M, Zitvogel L, Teng MWL, Belz GT, Engwerda CR, Huntington ND, Nakamura K, Hölzel M, Smyth MJ, Tumor immunoevasion by the conversion of effector NK cells into type 1 innate lymphoid cells, Nature immunology, 18 (2017) 1004–1015. [PubMed: 28759001]

[7]. Strait AA, Woolaver RA, Hall SC, Young CD, Karam SD, Jimeno A, Lan Y, Raben D, Wang JH, Wang X-J, Distinct immune microenvironment profiles of therapeutic responders emerge in combined TGFβ/PD-L1 blockade-treated squamous cell carcinoma, Communications Biology, 4 (2021) 1005. [PubMed: 34433873]

[8]. Tam S, Gross ND, Cutaneous Squamous Cell Carcinoma in Immunosuppressed Patients, Curr Oncol Rep, 21 (2019) 82. [PubMed: 31359288]

[9]. Elghouche AN, Pflum ZE, Schmalbach CE, Immunosuppression Impact on Head and Neck Cutaneous Squamous Cell Carcinoma: A Systematic Review with Meta-analysis, Otolaryngol Head Neck Surg, 160 (2019) 439–446. [PubMed: 30348055]

[10]. Chan MK-K, Chung JY-F, Tang PC-T, Chan AS-W, Ho JY-Y, Lin TP-T, Chen J, Leung K-T, To K-F, Lan H-Y, Tang PM-K, TGF-β signaling networks in the tumor microenvironment, Cancer Lett, 550 (2022) 215925. [PubMed: 36183857]

[11]. Chen T-W, Hung W-Z, Chiang S-F, Chen WT-L, Ke T-W, Liang J-A, Huang C-Y, Yang P-C, Huang KC-Y, Chao KSC, Dual inhibition of TGFβ signaling and CSF1/CSF1R reprograms tumor-infiltrating macrophages and improves response to chemotherapy via suppressing PD-L1, Cancer Lett, 543 (2022) 215795. [PubMed: 35718267]

[12]. Shi X, Luo J, Weigel KJ, Hall SC, Du D, Wu F, Rudolph MC, Zhou H, Young CD, Wang XJ, Cancer-Associated Fibroblasts Facilitate Squamous Cell Carcinoma Lung Metastasis in Mice by Providing TGFβ-Mediated Cancer Stem Cell Niche, Frontiers in cell and developmental biology, 9 (2021) 668164. [PubMed: 34527666]

[13]. Pang Y, Gara SK, Achyut BR, Li Z, Yan HH, Day CP, Weiss JM, Trinchieri G, Morris JC, Yang L, TGF-β signaling in myeloid cells is required for tumor metastasis, Cancer Discov, 3 (2013) 936–951. [PubMed: 23661553]

[14]. Mantovani A, Marchesi F, Jaillon S, Garlanda C, Allavena P, Tumor-associated myeloid cells: diversity and therapeutic targeting, Cellular & molecular immunology, 18 (2021) 566–578. [PubMed: 33473192]

[15]. Gabrilovich DI, Ostrand-Rosenberg S, Bronte V, Coordinated regulation of myeloid cells by tumours, Nat Rev Immunol, 12 (2012) 253–268. [PubMed: 22437938]

[16]. Zhou X, Fang D, Liu H, Ou X, Zhang C, Zhao Z, Zhao S, Peng J, Cai S, He Y, Xu J, PMN-MDSCs accumulation induced by CXCL1 promotes CD8+ T cells exhaustion in gastric cancer, Cancer Lett., 532 (2022) 215598. [PubMed: 35176418]

[17]. Kim IS, Gao Y, Welte T, Wang H, Liu J, Janghorban M, Sheng K, Niu Y, Goldstein A, Zhao N, Bado I, Lo HC, Toneff MJ, Nguyen T, Bu W, Jiang W, Arnold J, Gu F, He J, Jebakumar D, Walker K, Li Y, Mo Q, Westbrook TF, Zong C, Rao A, Sreekumar A, Rosen JM, Zhang XH, Immuno-subtyping of breast cancer reveals distinct myeloid cell profiles and immunotherapy resistance mechanisms, Nature cell biology, 21 (2019) 1113–1126. [PubMed: 31451770]

[18]. Swierczak A, Pollard JW, Myeloid Cells in Metastasis, Cold Spring Harbor perspectives in medicine, 10 (2020).

[19]. Umansky V, Adema GJ, Baran J, Brandau S, Van Ginderachter JA, Hu X, Jablonska J, Mojsilovic S, Papadaki HA, Pico de Coaña Y, Santegoets KCM, Santibanez JF, Serre K, Si Y, Sieminska I, Velegraki M, Fridlender ZG, Interactions among myeloid regulatory cells in cancer, Cancer immunology, immunotherapy : CII, 68 (2019) 645–660.

[20]. Wu FL, Nolan K, Strait AA, Bian L, Nguyen KA, Wang JH, Jimeno A, Zhou HM, Young CD, Wang XJ, Macrophages Promote Growth of Squamous Cancer Independent of T cells, J Dent Res, 98 (2019) 896–903. [PubMed: 31189369]

[21]. Vannini F, Kashfi K, Nath N, The dual role of iNOS in cancer, Redox biology, 6 (2015) 334–343. [PubMed: 26335399]

[22]. White RA, Neiman JM, Reddi A, Han G, Birlea S, Mitra D, Dionne L, Fernandez P, Murao K, Bian L, Keysar SB, Goldstein NB, Song N, Bornstein S, Han Z, Lu X, Wisell J, Li F, Song J, Lu SL, Jimeno A, Roop DR, Wang XJ, Epithelial stem cell mutations that promote squamous cell carcinoma metastasis, J Clin Invest, 123 (2013) 4390–4404. [PubMed: 23999427]

[23]. Li T, Li X, Zamani A, Wang W, Lee CN, Li M, Luo G, Eiler E, Sun H, Ghosh S, Jin J, Murali R, Ruan Q, Shi W, Chen YH, c-Rel Is a Myeloid Checkpoint for Cancer Immunotherapy, Nature cancer, 1 (2020) 507–517. [PubMed: 33458695]

[24]. Wang G, Lu X, Dey P, Deng P, Wu CC, Jiang S, Fang Z, Zhao K, Konaparthi R, Hua S, Zhang J, Li-Ning-Tapia EM, Kapoor A, Wu CJ, Patel NB, Guo Z, Ramamoorthy V, Tieu TN, Heffernan T, Zhao D, Shang X, Khadka S, Hou P, Hu B, Jin EJ, Yao W, Pan X, Ding Z, Shi Y, Li L, Chang Q, Troncoso P, Logothetis CJ, McArthur MJ, Chin L, Wang YA, DePinho RA, Targeting YAP-Dependent MDSC Infiltration Impairs Tumor Progression, Cancer Discov, 6 (2016) 80–95. [PubMed: 26701088]

[25]. Hanoteau A, Newton JM, Krupar R, Huang C, Liu HC, Gaspero A, Gartrell RD, Saenger YM, Hart TD, Santegoets SJ, Laoui D, Spanos C, Parikh F, Jayaraman P, Zhang B, Van der Burg SH, Van Ginderachter JA, Melief CJM, Sikora AG, Tumor microenvironment modulation enhances immunologic benefit of chemoradiotherapy, Journal for immunotherapy of cancer, 7 (2019) 10. [PubMed: 30646957]

[26]. Jayaraman P, Parikh F, Lopez-Rivera E, Hailemichael Y, Clark A, Ma G, Cannan D, Ramacher M, Kato M, Overwijk WW, Chen SH, Umansky VY, Sikora AG, Tumor expressed inducible nitric oxide synthase controls induction of functional myeloid-derived suppressor cells through modulation of vascular endothelial growth factor release, J Immunol, 188 (2012) 5365–5376. [PubMed: 22529296]

[27]. Lu G, Zhang R, Geng S, Peng L, Jayaraman P, Chen C, Xu F, Yang J, Li Q, Zheng H, Shen K, Wang J, Liu X, Wang W, Zheng Z, Qi CF, Si C, He JC, Liu K, Lira SA, Sikora AG, Li L, Xiong H, Myeloid cell-derived inducible nitric oxide synthase suppresses M1 macrophage polarization, Nat Commun, 6 (2015) 6676. [PubMed: 25813085]

[28]. Hoot KE, Lighthall J, Han G, Lu SL, Li A, Ju W, Kulesz-Martin M, Bottinger E, Wang XJ, Keratinocyte-specific Smad2 ablation results in increased epithelial-mesenchymal transition during skin cancer formation and progression, J Clin Invest, 118 (2008) 2722–2732. [PubMed: 18618014]

[29]. Fukumura D, Kashiwagi S, Jain RK, The role of nitric oxide in tumour progression, Nature reviews. Cancer, 6 (2006) 521–534. [PubMed: 16794635]

[30]. Kaczanowska S, Beury DW, Gopalan V, Tycko AK, Qin H, Clements ME, Drake J, Nwanze C, Murgai M, Rae Z, Ju W, Alexander KA, Kline J, Contreras CF, Wessel KM, Patel S, Hannenhalli S, Kelly MC, Kaplan RN, Genetically engineered myeloid cells rebalance the core immune suppression program in metastasis, Cell, 184 (2021) 2033–2052.e2021. [PubMed: 33765443]

[31]. Linde N, Casanova-Acebes M, Sosa MS, Mortha A, Rahman A, Farias E, Harper K, Tardio E, Reyes Torres I, Jones J, Condeelis J, Merad M, Aguirre-Ghiso JA, Macrophages orchestrate breast cancer early dissemination and metastasis, Nat Commun, 9 (2018) 21. [PubMed: 29295986]

[32]. Yan HH, Pickup M, Pang Y, Gorska AE, Li Z, Chytil A, Geng Y, Gray JW, Moses HL, Yang L, Gr-1+CD11b+ myeloid cells tip the balance of immune protection to tumor promotion in the premetastatic lung, Cancer research, 70 (2010) 6139–6149. [PubMed: 20631080]

[33]. Ortiz-Espinosa S, Morales X, Senent Y, Alignani D, Tavira B, Macaya I, Ruiz B, Moreno H, Remírez A, Sainz C, Rodriguez-Pena A, Oyarbide A, Ariz M, Andueza MP, Valencia K,

Teijeira A, Hoehlig K, Vater A, Rolfe B, Woodruff TM, Lopez-Picazo JM, Vicent S, Kochan G, Escors D, Gil-Bazo I, Perez-Gracia JL, Montuenga LM, Lambris JD, Ortiz de Solorzano C, Lecanda F, Ajona D, Pio R, Complement C5a induces the formation of neutrophil extracellular traps by myeloid-derived suppressor cells to promote metastasis, Cancer Lett, 529 (2022) 70–84. [PubMed: 34971753]

[34]. Elmusrati A, Wang J, Wang CY, Tumor microenvironment and immune evasion in head and neck squamous cell carcinoma, Int J Oral Sci, 13 (2021) 24. [PubMed: 34341329]

[35]. Bian K, Ghassemi F, Sotolongo A, Siu A, Shauger L, Kots A, Murad F, NOS-2 signaling and cancer therapy, IUBMB Life, 64 (2012) 676–683. [PubMed: 22715033]

[36]. Chung AW, Anand K, Anselme AC, Chan AA, Gupta N, Venta LA, Schwartz MR, Qian W, Xu Y, Zhang L, Kuhn J, Patel T, Rodriguez AA, Belcheva A, Darcourt J, Ensor J, Bernicker E, Pan PY, Chen SH, Lee DJ, Niravath PA, Chang JC, A phase 1/2 clinical trial of the nitric oxide synthase inhibitor L-NMMA and taxane for treating chemoresistant triple-negative breast cancer, Science translational medicine, 13 (2021) eabj5070. [PubMed: 34910551]

[37]. Gallo O, Masini E, Morbidelli L, Franchi A, Fini-Storchi I, Vergari WA, Ziche M, Role of nitric oxide in angiogenesis and tumor progression in head and neck cancer, Journal of the National Cancer Institute, 90 (1998) 587–596. [PubMed: 9554441]

[38]. Brennan PA, Palacios-Callender M, Zaki GA, Spedding AV, Langdon JD, Type II nitric oxide synthase (NOS2) expression correlates with lymph node status in oral squamous cell carcinoma, Journal of oral pathology & medicine : official publication of the International Association of Oral Pathologists and the American Academy of Oral Pathology, 30 (2001) 129–134. [PubMed: 11271626]

[39]. Trovato R, Cane S, Petrova V, Sartoris S, Ugel S, De Sanctis F, The Engagement Between MDSCs and Metastases: Partners in Crime, Front Oncol, 10 (2020) 165. [PubMed: 32133298]

[40]. Kessenbrock K, Plaks V, Werb Z, Matrix metalloproteinases: regulators of the tumor microenvironment, Cell, 141 (2010) 52–67. [PubMed: 20371345]

[41]. Spicer JD, McDonald B, Cools-Lartigue JJ, Chow SC, Giannias B, Kubes P, Ferri LE, Neutrophils promote liver metastasis via Mac-1-mediated interactions with circulating tumor cells, Cancer research, 72 (2012) 3919–3927. [PubMed: 22751466]

[42]. Szczerba BM, Castro-Giner F, Vetter M, Krol I, Gkountela S, Landin J, Scheidmann MC, Donato C, Scherrer R, Singer J, Beisel C, Kurzeder C, Heinzelmann-Schwarz V, Rochlitz C, Weber WP, Beerenwinkel N, Aceto N, Neutrophils escort circulating tumour cells to enable cell cycle progression, Nature, 566 (2019) 553–557. [PubMed: 30728496]

[43]. Sikora AG, Gelbard A, Davies MA, Sano D, Ekmekcioglu S, Kwon J, Hailemichael Y, Jayaraman P, Myers JN, Grimm EA, Overwijk WW, Targeted inhibition of inducible nitric oxide synthase inhibits growth of human melanoma in vivo and synergizes with chemotherapy, Clinical cancer research : an official journal of the American Association for Cancer Research, 16 (2010) 1834–1844.

[44]. Belgorosky D, Girouard J, Langle YV, Hamelin-Morrissete J, Marino L, Agüero EI, Malagrino H, Reyes-Moreno C, Eiján AM, Relevance of iNOS expression in tumor growth and maintenance of cancer stem cells in a bladder cancer model, Journal of molecular medicine (Berlin, Germany), 98 (2020) 1615–1627. [PubMed: 32955679]

[45]. Gallorini M, Maccallini C, Ammazzalorso A, Amoia P, De Filippis B, Fantacuzzi M, Giampietro L, Cataldi A, Amoroso R, The Selective Acetamidine-Based iNOS Inhibitor CM544 Reduces Glioma Cell Proliferation by Enhancing PARP-1 Cleavage In Vitro, International journal of molecular sciences, 20 (2019).

[46]. Matsumoto G, Muta M, Tsuruta K, Horiguchi S, Karasawa K, Okamoto A, Tumor size significantly correlates with postoperative liver metastases and COX-2 expression in patients with resectable pancreatic cancer, Pancreatology : official journal of the International Association of Pancreatology (IAP) … [et al.], 7 (2007) 167–173.

[47]. Forsthuber A, Lipp K, Andersen L, Ebersberger S, Graña C, Ellmeier W, Petzelbauer P, Lichtenberger BM, Loewe R, CXCL5 as Regulator of Neutrophil Function in Cutaneous Melanoma, The Journal of investigative dermatology, 139 (2019) 186–194. [PubMed: 30009831]

[48]. Zhang W, Wang H, Sun M, Deng X, Wu X, Ma Y, Li M, Shuoa SM, You Q, Miao L, CXCL5/CXCR2 axis in tumor microenvironment as potential diagnostic biomarker and therapeutic target, Cancer Commun (Lond), 40 (2020) 69–80. [PubMed: 32237072]

- SCC lung metastasis depended upon iNOS and $Gr1^+$ myeloid cells activated by TGFβ
- L-NIL inhibited SCC lung metastasis with reductions of myeloid cells and Cxcl5
- TGFβ inhibitor, anti-Gr1, L-NIL, and Cxcr2 inhibitor all reduced lung metastasis

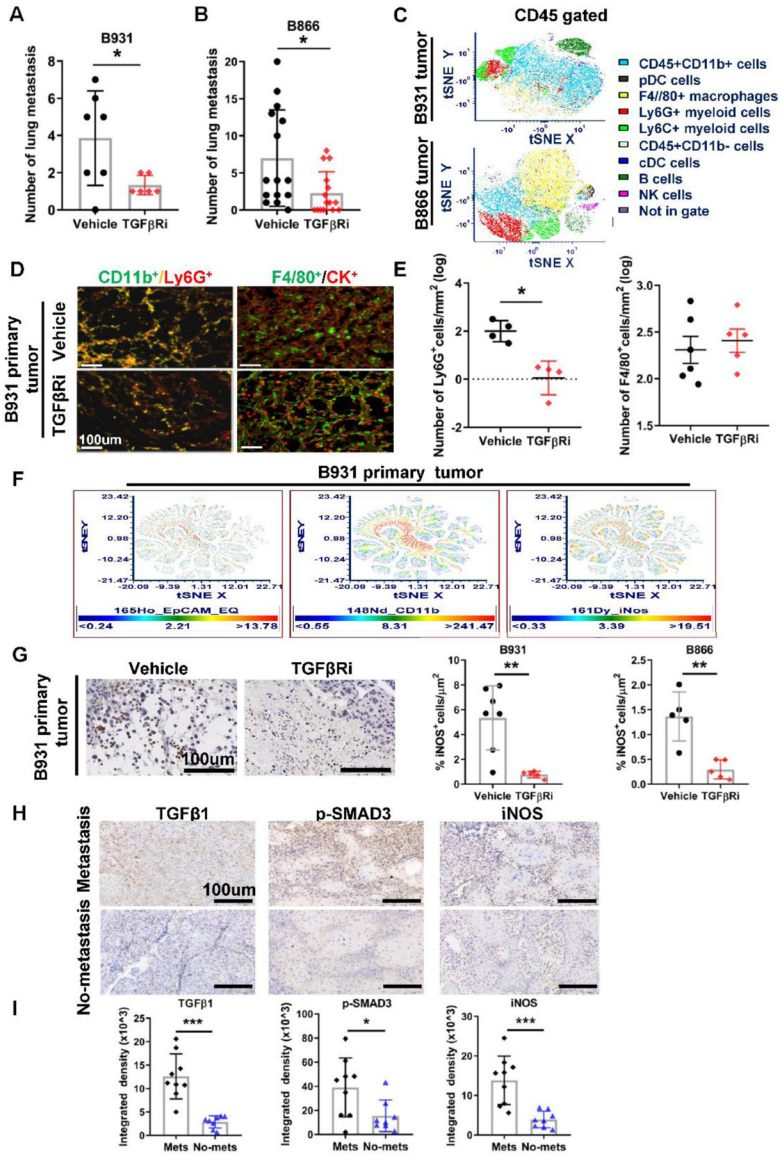

Fig.1. TGFβR inhibitor reduced lung metastasis correlating to reduced CD11b$^+$/Gr1$^+$ myeloid cells and iNOS$^+$ cells.

A-B, Quantification of lung metastasis of B931 and B866 tumor bearing mice comparing TGFβR inhibitor (TGFβRi) with vehicle treated groups (B931, n=7 of vehicle and n=6 of TGFβRi group; B866, n=15/group). C, CD45$^+$ immune cell populations of B931 (upper panel) and B866 (lower panel) primary tumors using CyTOF analysis and tSNE clustering, tSNE plots displaying immune cell subset identification overlay plots. D, Representative images of CD11b, Ly6G, F4/80 and cytokeratin (CK) staining in primary B931 tumors treated with TGFβRi or vehicle. E, Number of CD11b$^+$Ly6G$^+$ cells was quantified per primary tumor (n=4/group). Number of F4/80$^+$ cells was quantified per primary tumor (n=6 of vehicle and n=5 of TGFβRi group). F, Levels of Epcam, CD11b and iNOS in dissociated B931 primary tumors analyzed by CyTOF, color represents the intensity of expression level (blue: low; red: high). G, Representative IHC images of iNOS$^+$ staining in B931 primary tumors treated with vehicle or TGFβRi. Quantification of iNOS$^+$ cells in B931 and B866

primary tumors from mice treated with TGFβRi or vehicle (B931, n=7 of vehicle and n=5 of TGFβRi group; B866, n=5/group).H, Representative IHC images of indicated markers in human OSCC. Upper panels are staining of the primary tumor of a patient with metastasis and lower panels are staining of the primary tumor from a representative patient without metastasis; I, Quantification of TGFβ1, p-SMAD3, and iNOS staining (n=9 of metastasis and n=8 of no-metastasis group).

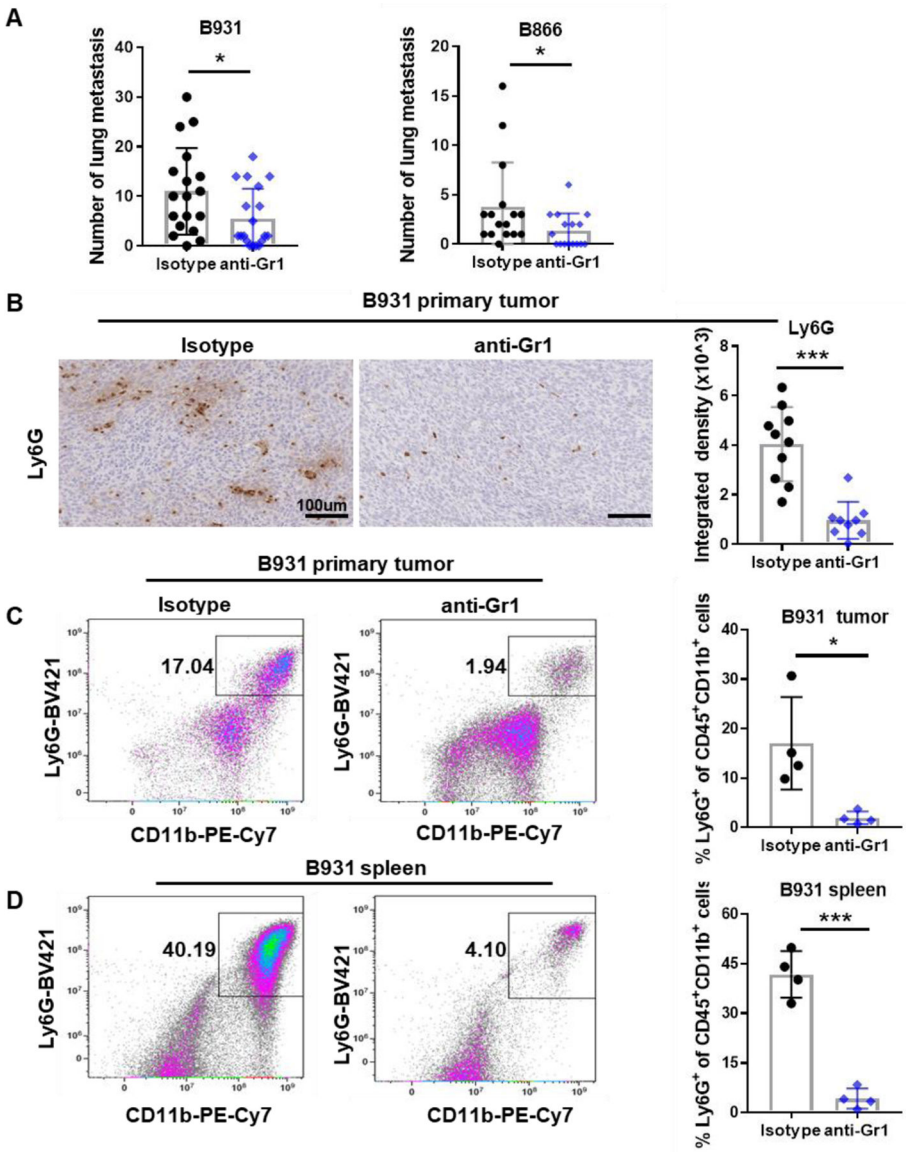

Fig.2. Gr1+ myeloid cell depletion reduced SCC lung metastasis.

A, Number of lung metastasis of isotype and anti-Gr1 treated B931 and B866 tumor bearing mice (B931, n=18 of isotype and n=19 of anti-Gr1 group; B866, n=15/group). B, Representative IHC images stained for Ly6G in B931 primary tumors from mice treated with isotype control or anti-Gr1 antibody and quantification (n=10 of isotype and n=9 of anti-Gr1 group). C, Representative B931 flow cytometry of dissociated B931 tumors to determine CD11b+ Ly6G+ subsets (gated on upstream live, CD45+ events) in tumors treated with isotype control or anti-Gr1 antibody and quantification (n=4/group). D, Representative flow cytometry of spleens to determine CD11b+ Ly6G+ subsets (gated on upstream live, CD45+ events) treated with isotype control or anti-Gr1 antibody and percentage of Ly6G+ cells (n=4/group).

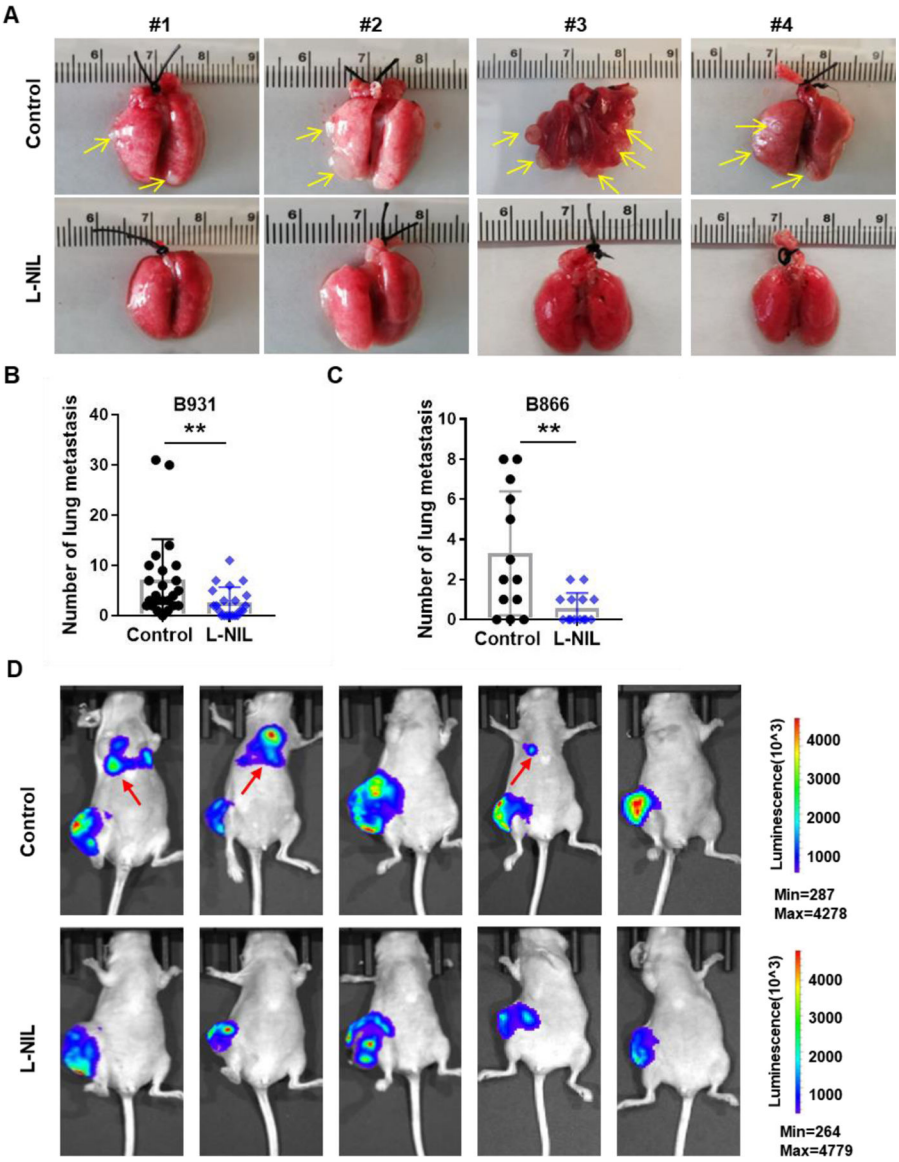

Fig.3. iNOS inhibitor reduced SCC lung metastasis.

A, Representative gross lung metastasis images in mice bearing B931 tumors treated with L-NIL versus control. B-C, Quantification of lung metastasis number in mice bearing B931 (A) or B866 (B) tumors treated with L-NIL verse control (B931, n=24 of control and n=21 of L-NIL group; B866, n=13/group). D, Bioluminescence imaging of B931 tumor bearing mice at 5 weeks post tumor injection (red arrows indicate lung metastasis).

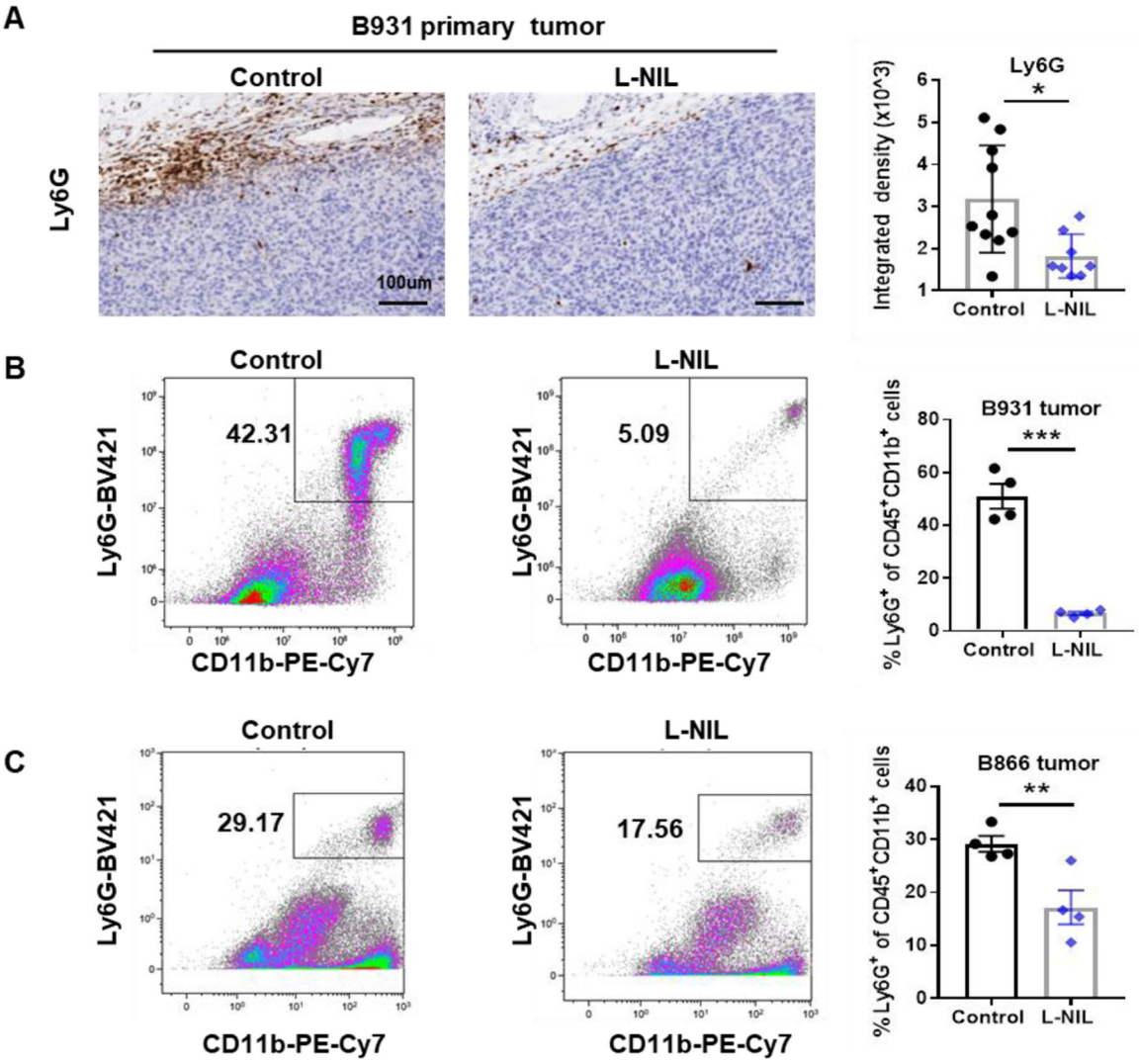

Fig.4. Ly6G$^+$ myeloid cells were reduced in tumors from mice treated with L-NIL.

A, Representative IHC staining of Ly6G in primary tumors from B931 tumor bearing mice treated with L-NIL or control. Quantification of staining on the right (n=10 of control and n=8 of L-NIL group). B-C, Representative flow cytometry of dissociated B931 (B) and B866 tumors (C) to determine CD11b$^+$ Ly6G$^+$ subsets (gated on upstream live, CD45+ events) and quantification of the percentage of Ly6G$^+$ myeloid cells in B931 and B866 tumors from mice treated with control or L-NIL (n=4/group).

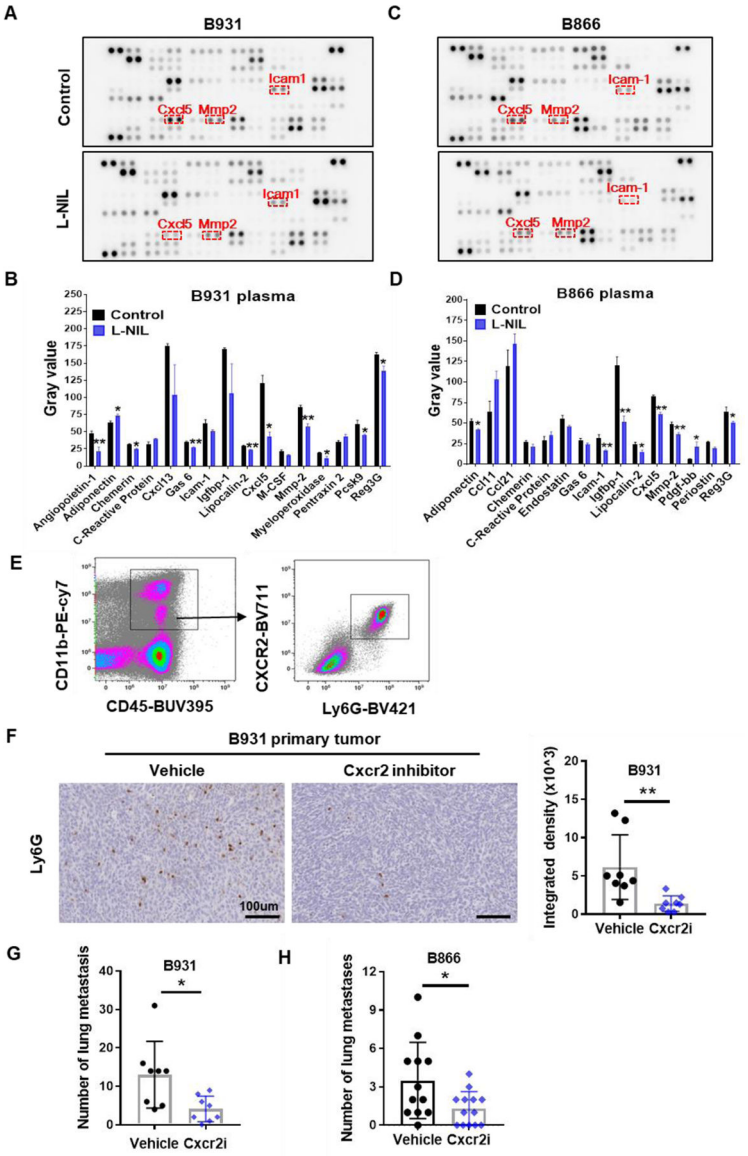

Fig.5. Cxcl5 is a major L-NIL target and Cxcl5/Cxcr2 inhibition reduced SCC lung metastasis. A and C, Representative cytokine array images of plasma samples from control or L-NIL treated mice bearing B931 tumors (A) or B866 tumors (C). B and D, Quantification of cytokine array mean gray values in plasma from mice bearing B931(B) or B866 tumors (D) (n=4/group). E, Cxcr2 expression in Ly6G^{+} cells (gated on live, CD45+, CD11b+ cells) in B931 primary tumor was detected by flow cytometry. F, Representative images of Ly6G IHC staining and quantification in B931 primary tumors from control or Cxcr2 inhibitor (Cxcr2i) treated mice (n=8/group). G-H, Number of lung metastasis from vehicle and Cxcr2 inhibitor (Cxcr2i) treated B931 and B866 tumor bearing mice (B931, n=8/group; B866, n=12 of vehicle and n=13 of Cxcr2 inhibitor group).

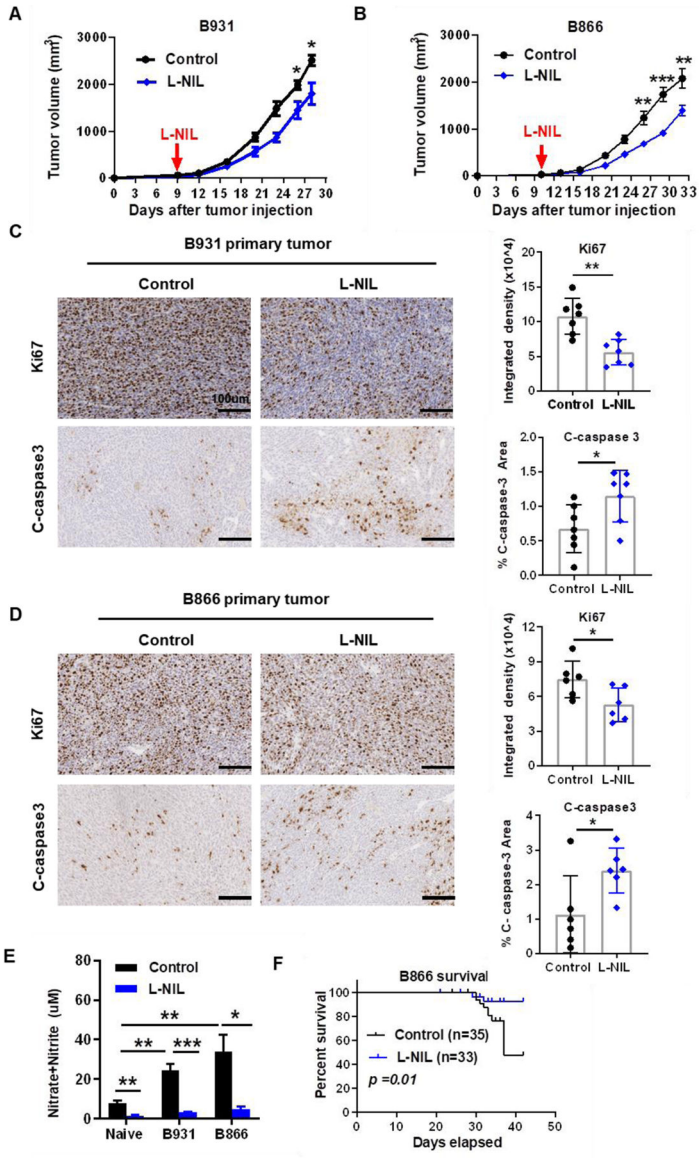

Fig.6. L-NIL inhibited tumor growth, reduced proliferation and promoted apoptosis.

A-B, Tumor volume in control and L-NIL treated B931 (A) and B866 (B) mice (B931, n=9/group; B866, n=15/group). C-D, Representative Ki67 and cleaved-caspase3 IHC stained images and quantification of B931 (C) and B866 primary tumors (D) from control and L-NIL treated mice (B931, n=7/group; B866, n=6/group). E, Nitrate and nitrite levels in the plasma of naïve, B931- or B866-tumor bearing mice treated with control or L-NIL (n=4/group). F, Kaplan–Meier survival analysis of B866 tumor bearing mice treated with control or L-NIL （n=35 of control and n=33 of L-NIL group, the data were combined for survival analysis from two independent experiments）

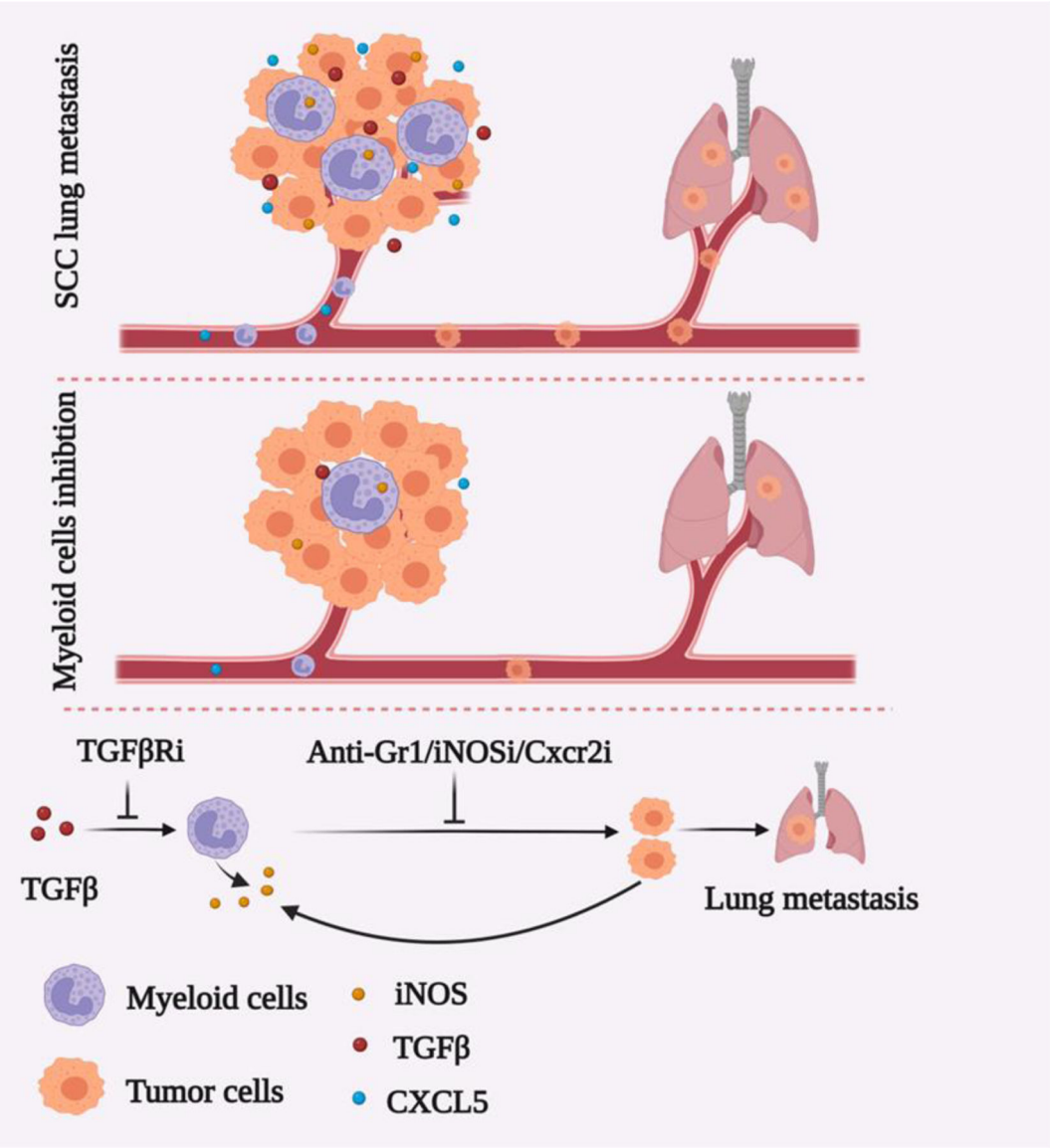

Fig.7. Model of regulatory mechanism and function of TGFβ in OSCC lung metastasis.
iNOS and Gr1+ myeloid cells are major contributors to TGFβ-mediated lung metastasis. iNOS inhibitor L-NIL inhibited SCC lung metastasis with the mechanism associated with reducing Cxcl5 induced myeloid cell infiltration.